J. Fluid Mech. (2021), *vol*. 923, R5, doi:10.1017/jfm.2021.621

Flow rate–pressure drop relation for shear-thinning fluids in narrow channels: approximate solutions and comparison with experiments

Evgeniy Boyko[1],† **and Howard A. Stone**[1],†

[1]Department of Mechanical and Aerospace Engineering, Princeton University, Princeton, NJ 08544, USA

(Received 18 May 2021; revised 28 June 2021; accepted 2 July 2021)

Non-Newtonian fluids are characterized by complex rheological behaviour that affects the hydrodynamic features, such as the flow rate–pressure drop relation. While flow rate–pressure drop measurements of such fluids are common in the literature, a comparison of experimental data with theory is rare, even for shear-thinning fluids at low Reynolds number, presumably due to the lack of analytical expressions for the flow rate–pressure drop relation covering the entire range of pressures and flow rates. Such a comparison, however, is of fundamental importance as it may provide insight into the adequacy of the constitutive model that was used and the values of the rheological parameters. In this work, we present a theoretical approach to calculating the flow rate–pressure drop relation of shear-thinning fluids in long, narrow channels that can be used for comparison with experimental measurements. We utilize the Carreau constitutive model and provide a semi-analytical expression for the flow rate–pressure drop relation. In particular, we derive three asymptotic solutions for small, intermediate and large values of the dimensionless pressures or flow rates, which agree with distinct limits previously known and allow us to approximate analytically the entire flow rate–pressure drop curve. We compare our semi-analytical and asymptotic results with the experimental measurements of Pipe *et al.* (*Rheol. Acta*, vol. 47, 2008, pp. 621–642) and find excellent agreement. Our results rationalize the change in the slope of the flow rate–pressure drop data, when reported in log–log coordinates, at high flow rates, which cannot be explained using a simple power-law model.

Key words: non-Newtonian flows, rheology, low-Reynolds-number flows

† Email addresses for correspondence: eboyko@princeton.edu, hastone@princeton.edu

1. Introduction

One might think that obtaining analytical expressions, even approximate ones, for the relationship between the pressure drop Δp across a channel and the flow rate q at low Reynolds number is no more than a theoretical exercise and can be found in standard textbooks. While certainly true for the laminar flow of Newtonian fluids for common geometries, with the result displaying a well-known linear $q-\Delta p$ relation (Happel & Brenner 1983; Sutera & Skalak 1993), answers are not so straightforward for the flow of non-Newtonian fluids, for which nonlinear relations between q and Δp should be expected.

Even for shear-thinning fluids with a shear-dependent viscosity at low Reynolds number, analytical expressions for the $q-\Delta p$ relation are available only for the power-law and Ellis models in simple geometries, such as capillaries and slit channels (see Bird, Armstrong & Hassager (1987), p. 229). One well-established approach to obtaining the $q-\Delta p$ relation of power-law fluids in capillaries and slit channels relies on the Weissenberg–Rabinowitsch–Mooney methodology (Rabinowitsch 1929; Mooney 1931; Macosko 1994). While such an approach applies to all generalized Newtonian fluids, following Metzner & Reed (1955) and Metzner (1957), it is widely used assuming the power-law rheology. However, both power-law and Ellis models are too simplistic and cannot adequately describe the variation of viscosity of common non-Newtonian fluids over the whole range of shear rates. In fact, both models fail to reproduce the high-shear-rate viscosity plateau, and the power-law model also fails to reproduce the low-shear-rate viscosity plateau and has a well-known singularity at zero shear rate (Bird *et al.* 1987). One of the models that resolves these issues and reproduces the realistic rheological behaviour of shear-thinning fluids over the entire range of shear rates is the Carreau (1972) constitutive model. To the best of our knowledge, however, no analytical solution for the $q-\Delta p$ relation of the Carreau model has been reported in the literature, even for simple geometries.

Recently, Sochi (2015) presented a semi-analytical $q-\Delta p$ relation for a Carreau fluid. Using the Weissenberg–Rabinowitsch–Mooney methodology, Sochi (2015) related q and Δp to an integral that can be expressed in terms of hypergeometric functions. However, since this integral depends on the wall shear rate $\dot{\gamma}_w$, which is not *a priori* known and must be obtained by numerically solving a nonlinear algebraic equation for a given Δp, the presented solution cannot be considered fully analytical; it is certainly inconvenient to use due to its complex form.

It should be noted that, due to its simplicity and despite its limitations, the power-law model has been widely used to obtain $q-\Delta p$ relations of shear-thinning fluids at low Reynolds number in various geometries, including expanding (Pinho, Oliveira & Miranda 2003) and elastic (Anand, David & Christov 2019) channels. However, several recent works that studied different hydrodynamic problems involving shear-thinning fluids at low Reynolds number clearly showed that a simple power-law model has a small range of applicability where it can reproduce the response obtained with the more realistic Ellis and Carreau models (Moukhtari & Lecampion 2018; Picchi *et al.* 2021). Therefore, one should be cautious when using the results based on the power-law rheology, especially at low and high shear rates.

A quantitative comparison of any analytical or numerical solution with experimental data is of fundamental importance in non-Newtonian fluid mechanics, since any such solution depends on the parameters of a constitutive model that cannot typically be evaluated precisely from experiments. Such a comparison may serve as a sanity check for the applicability of the solution and the values of rheological parameters. While measurements of q and Δp are widely conducted in capillary and microfluidic viscometry

to determine the shear-rate-dependent viscosity (Lodge & de Vargas 1983; Macosko 1994; Kang, Lee & Koelling 2005; Pipe & McKinley 2009; Gupta, Wang & Vanapalli 2016), comparison of experimental data on q and Δp with theory is rarely performed. Importantly, microchannel flows allow preservation of the small value of the Reynolds number and assessment of the viscosity at high shear rates, which cannot be measured by standard rheometers as these are limited to low and intermediate values of shear rates (Ewoldt, Johnston & Caretta 2015; Gupta *et al.* 2016). For example, Pipe, Majmudar & McKinley (2008) presented $q-\Delta p$ measurements of the shear-thinning xanthan gum solutions in a slit microchannel for a wide range of flow rates and converted these measurements into the shear-rate-dependent viscosity. Even though Pipe *et al.* (2008) fitted the viscosity data to the Carreau–Yasuda model, no comparison of the $q-\Delta p$ data with the theory based on the obtained viscosity distribution was presented. One possible reason for this may have been their interest in the solution viscosity rather than in the $q-\Delta p$ behaviour, which also explains why $q-\Delta p$ data are usually not presented in the viscometry literature. Such information, however, should be expected to be important to many applications. Moreover, in our opinion, another possible reason for the dearth of experiment/theory comparisons of $q-\Delta p$ data is the difficulty of performing such a comparison due to the lack of analytical expressions, even approximate ones, for the $q-\Delta p$ relation, which should be simple to use while also describing the entire range of pressures and flow rates.

In this work, we provide a theoretical framework for calculating the flow rate–pressure drop relation of shear-thinning fluids in long, narrow channels that can be used for comparison with experimental measurements. We present an alternative semi-analytical solution for the $q-\Delta p$ relation of Carreau fluids and use it to derive three asymptotic solutions for small, intermediate and large values of the (appropriate dimensionless) pressures or flow rates, which allows us to approximate analytically the entire $q-\Delta p$ curve. We then compare our semi-analytical and asymptotic solutions with the experimental measurements of Pipe *et al.* (2008), finding excellent agreement between the two. In addition, our calculations rationalize the change in the slope of the $q-\Delta p$ data, when reported in log–log coordinates, observed in the experiments of Pipe *et al.* (2008) at high flow rates. This change in the slope cannot be explained using a simple power-law model, thus highlighting the importance of choosing the appropriate rheological model for description of the flows of non-Newtonian fluids.

2. Problem formulation and governing equations

We study the incompressible steady pressure-driven flow of a non-Newtonian shear-thinning fluid in a channel of length ℓ_{ch}, width w and height h, where $h \ll w \ll \ell_{ch}$. We assume that the imposed flow rate q induces the fluid motion with velocity $\boldsymbol{u} = (u_x, u_y, u_z)$ and pressure distribution p. Motivated by the experimental set-up of Pipe *et al.* (2008), we assume that two pressure sensors, measuring the pressure drop Δp over a streamwise distance ℓ, are located far from the channel ends, where the flow is fully developed and the entrance and exit effects are negligible. Our primary interest is to determine the steady-state relation between the pressure drop Δp and the flow rate q. Figure 1 presents a schematic illustration of the flow configuration and the Cartesian coordinate system (x, y, z), in which the x- and y-axes lie in the midplane of the channel and z is in the direction of the shortest dimension.

We consider low-Reynolds-number flows, so that the fluid inertia is negligible relative to viscous stresses. In this limit, the fluid motion is governed by the continuity and

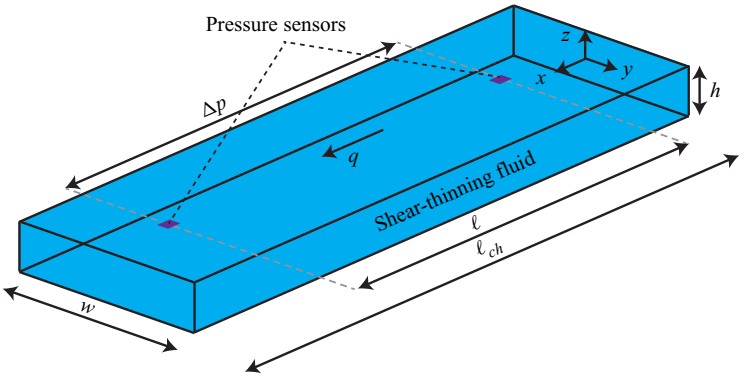

Figure 1. Schematic illustration of the flow configuration consisting of a channel of length ℓ_{ch}, width w and height h. The channel contains a shear-thinning fluid steadily driven by the imposed flow rate q. Our interest is to determine the pressure drop Δp over a streamwise distance ℓ between two pressure sensors located far from the channel entrance and exit.

momentum equations

$$\boldsymbol{\nabla \cdot u} = 0, \quad \boldsymbol{\nabla \cdot \sigma} = \boldsymbol{0}, \tag{2.1a,b}$$

where $\boldsymbol{\sigma}$ is the stress tensor. The description of the non-Newtonian fluid rheology requires the use of a specific constitutive equation for $\boldsymbol{\sigma}$. In this work, we consider the generalized Newtonian model, with $\boldsymbol{\sigma}$ given by (Bird *et al.* 1987)

$$\boldsymbol{\sigma} = -p\boldsymbol{I} + 2\eta(\dot{\gamma})\boldsymbol{E}, \tag{2.2}$$

where $\boldsymbol{E} = (\boldsymbol{\nabla u} + (\boldsymbol{\nabla u})^{\mathrm{T}})/2$ is the rate-of-strain tensor. The generalized Newtonian fluid follows the same form of the stress tensor as the Newtonian fluid and depends only on the instantaneous velocity and not on the flow history. However, the viscosity $\eta(\dot{\gamma})$ of the generalized Newtonian fluid depends on the shear rate $\dot{\gamma} = \sqrt{2\boldsymbol{E}:\boldsymbol{E}}$, in contrast to the familiar Newtonian fluid.

Throughout this work, we consider the Carreau model for $\eta(\dot{\gamma})$, which describes three experimentally observed behaviours of viscosity, namely, plateaus in viscosity at very low or very high shear rates and power-law dependence at intermediate shear rates. The constitutive description is given by (Bird *et al.* 1987; Morozov & Spagnolie 2015)

$$\eta(\dot{\gamma}) = \eta_\infty + (\eta_0 - \eta_\infty)(1 + (\lambda\dot{\gamma})^2)^{(n-1)/2}, \tag{2.3}$$

where η_0 and η_∞ are the zero- and infinite-shear-rate viscosities, respectively. The power-law index n characterizes the degree of shear thinning ($0 < n \leq 1$) and λ is the inverse of a characteristic shear rate at which shear thinning becomes apparent. The case of $n = 1$, $\lambda = 0$ or $\eta_0 = \eta_\infty$ represents the Newtonian fluid with a constant viscosity η_0. As noted by Bird *et al.* (1987), for $\eta_\infty = 0$ and high shear rates, $\lambda\dot{\gamma} \gg 1$, the Carreau model reduces to the well-known power-law model $\eta(\dot{\gamma}) = \eta_0\lambda^{n-1}\dot{\gamma}^{n-1}$. Since for most shear-thinning fluids $\eta_\infty/\eta_0 \ll 1$ but $\eta_\infty \neq 0$, the power-law model is expected to accurately capture the rheological behaviour only at intermediate values of the shear rate.

3. Theoretical analysis for narrow channels and the flow rate–pressure drop relation

3.1. *The velocity and viscosity distributions*

For long and narrow straight channels in which $h \ll w \ll \ell_{ch}$, we can assume a rectilinear flow, $\boldsymbol{u} = u_x(y, z)\boldsymbol{e}_x$. Furthermore, the assumption $h \ll w$ implies that $\partial/\partial y \ll \partial/\partial z$, so

that the momentum equations (2.1*b*) together with (2.2) simplify to

$$\frac{\partial p}{\partial x} = \frac{\partial}{\partial z}\left(\eta(\dot\gamma)\frac{\partial u_x}{\partial z}\right), \quad \frac{\partial p}{\partial y} = 0, \quad \frac{\partial p}{\partial z} = 0, \quad \text{with } \dot\gamma = \left|\frac{\partial u_x}{\partial z}\right|. \tag{3.1a–d}$$

We note that the governing equations (3.1) represent the lubrication equations and can be derived alternatively by introducing two small parameters $\epsilon = h/\ell_{ch} \ll 1$ and $\delta = h/w \ll 1$, with the ordering $0 < \epsilon \ll \delta \ll 1$, and then formally expanding the velocity and pressure fields in powers of ϵ and δ, keeping finally the leading-order terms (see e.g. Christov *et al.* 2018). From (3.1*b*,*c*), it follows that $p = p(x)$, i.e. the pressure is independent of y and z, consistent with the classical lubrication approximation.

Integrating (3.1*a*) with respect to z and applying the symmetry condition at the midplane yields

$$\frac{\mathrm{d}p}{\mathrm{d}x} z = \eta(\dot\gamma)\frac{\partial u_x}{\partial z}. \tag{3.2}$$

For a straight channel, the pressure gradient is constant and can be expressed as $\mathrm{d}p/\mathrm{d}x = -\Delta p/\ell$, leading to

$$\frac{\partial u_x}{\partial z} = -\frac{\Delta p}{\ell}\frac{z}{\eta(\dot\gamma)}, \tag{3.3}$$

so that the shear rate is $\dot\gamma = z\Delta p/(\eta(\dot\gamma)\ell)$. Substituting the latter result into the constitutive equation for η results in an implicit nonlinear algebraic equation for the viscosity distribution η. The Carreau model, (2.3), takes the dimensionless form

$$\frac{\eta}{\eta_0} = \beta + (1-\beta)\left(1 + \left(\frac{CuZ}{\eta/\eta_0}\right)^2\right)^{(n-1)/2}, \tag{3.4}$$

where $\beta = \eta_\infty/\eta_0$, $Z = z/h$ and Cu is the Carreau number (see e.g. Datt *et al.* 2015; Shahsavari & McKinley 2015), defined for convenience based on the pressure drop Δp rather than on the flow rate q as

$$Cu = \frac{\lambda\Delta p}{\eta_0}\frac{h}{\ell}. \tag{3.5}$$

Integrating (3.3) again with respect to z and applying the no-slip boundary conditions at the channel walls, we obtain the axial velocity $u_x = -(\Delta p/\ell)\int_{h/2}^{z} z'\eta(z')^{-1}\,\mathrm{d}z'$. Substituting this result into the definition of the volumetric flow rate q through the microchannel, $q = 2\int_{-w/2}^{w/2}\int_0^{h/2} u_x(z)\,\mathrm{d}z\,\mathrm{d}y$, gives the flow rate–pressure drop relation

$$q = -\frac{2(\Delta p)w}{\ell}\int_0^{h/2}\int_{h/2}^{z}\frac{z'}{\eta(z')}\,\mathrm{d}z'\,\mathrm{d}z, \tag{3.6}$$

which requires first solving for the viscosity distribution η using (3.4). Defining $Q = q/(wh^2/\lambda)$, the flow rate–pressure drop relation (3.6) can be expressed in a non-dimensional form in terms of the Carreau number,

$$Q = -2Cu\int_0^{1/2}\int_{1/2}^{Z} Z'(\eta(Z')/\eta_0)^{-1}\,\mathrm{d}Z'\,\mathrm{d}Z. \tag{3.7}$$

While no general closed-form analytical solution of (3.4) and (3.7) is available, we next provide three asymptotic solutions in the limit of small, intermediate and large values

of Cu, which allow us to describe analytically almost the entire range of values of the Carreau number.

We note that our approach to calculating the $q-\Delta p$ relation (3.7) differs from that of Sochi (2015), which relies on the Weissenberg–Rabinowitsch–Mooney methodology and eliminates the need to find the velocity profile, relating q and Δp to the *a priori* unknown wall shear rate $\dot{\gamma}_w$ via hypergeometric functions.

3.2. *Asymptotic results for small, intermediate and large values of Cu*

For weak actuation, corresponding to the limit $Cu \ll 1$, the viscosity is $\eta/\eta_0 = 1$ at the leading order, and Q scales linearly with the Carreau number, $Q = Cu/12$. To determine the $q-\Delta p$ relation at higher orders, we seek the viscosity function in the form $\eta/\eta_0 = 1 + Cu^2\mathcal{H}_1 + Cu^4\mathcal{H}_2 + O(Cu^6)$. Substituting this expansion into (3.4) and solving order by order, we obtain

$$\mathcal{H}_1 = -\tfrac{1}{2}(1-n)(1-\beta)Z^2, \quad \mathcal{H}_2 = -\tfrac{1}{8}(1-n)(1-\beta)(1-3n+4(n-1)\beta)Z^4. \tag{3.8a,b}$$

Using (3.8) and approximating $(\eta/\eta_0)^{-1}$ as $(\eta/\eta_0)^{-1} = 1 - Cu^2\mathcal{H}_1 + Cu^4(\mathcal{H}_1^2 - \mathcal{H}_2)$, the flow rate–pressure drop relation (3.7) takes the form

$$Q = \frac{Cu}{12} + \frac{(1-n)(1-\beta)Cu^3}{160} + \frac{(1-n)(1-\beta)(3-5n+6(n-1)\beta)Cu^5}{3584} + O(Cu^7) \quad \text{for } Cu \ll 1. \tag{3.9}$$

For intermediate values of Cu, under the assumption of $\beta = \eta_\infty/\eta_0 \ll 1$, which holds for most shear-thinning fluids, the Carreau model (2.3) reduces to a power-law model with $\eta/\eta_0 = (CuZ)^{(n-1)/n}$, which has a well-known singularity at $Z = 0$ for $0 < n < 1$. Nevertheless, since the integrand $Z(\eta(Z)/\eta_0)^{-1} \propto Z^{1/n}$ of (3.7) is a regular function for $Z \in [0, 1/2]$, the integration in (3.7) can be calculated, leading to the well-known $q-\Delta p$ relation (see e.g. Bird *et al.* (1987), p. 176)

$$Q = \frac{n}{2n+1}\frac{Cu^{1/n}}{2^{(n+1)/n}} \quad \text{for intermediate } Cu. \tag{3.10}$$

For strong actuation, corresponding to the limit $Cu \gg 1$, we approximate the viscosity (3.4) as $\eta/\eta_0 = \beta + (1-\beta)(Cu(\eta/\eta_0)^{-1}Z)^{n-1}$, so that $\eta/\eta_0 = \beta$ at the leading order, and Q again scales linearly with the Carreau number, $Q = Cu/(12\beta)$. To determine high-order solutions, we seek the viscosity function in the form $\eta/\eta_0 = \beta + Cu^{n-1}\mathcal{H}_1 + Cu^{2(n-1)}\mathcal{H}_2 + O(Cu^{3(n-1)})$, satisfying $Cu^{2(n-1)} \ll Cu^{n-1} \ll 1$, which is strictly valid for shear-thinning fluids with $0 < n < 1$. Substituting this expansion into the approximate expression for viscosity, we obtain

$$\mathcal{H}_1 = (1-\beta)\left(\frac{Z}{\beta}\right)^{n-1}, \quad \mathcal{H}_2 = \frac{(1-n)(1-\beta)^2}{\beta}\left(\frac{Z}{\beta}\right)^{2n-2}. \tag{3.11a,b}$$

Using (3.11) and approximating $(\eta/\eta_0)^{-1}$ as $(\eta/\eta_0)^{-1} = \beta^{-1} - \beta^{-2}Cu^{n-1}\mathcal{H}_1 + \beta^{-3}Cu^{2(n-1)}(\mathcal{H}_1^2 - \beta\mathcal{H}_2)$, the flow rate–pressure drop relation (3.7) in the limit $Cu \gg 1$ is

$$Q = \frac{Cu}{12\beta} - \frac{(1-\beta)Cu^n}{2^{n+1}\beta^{n+1}(n+2)} + \frac{n(1-\beta)^2Cu^{2n-1}}{2^{2n}\beta^{2n+1}(2n+1)} + O(Cu^{3n-2}) \quad \text{for } Cu \gg 1. \tag{3.12}$$

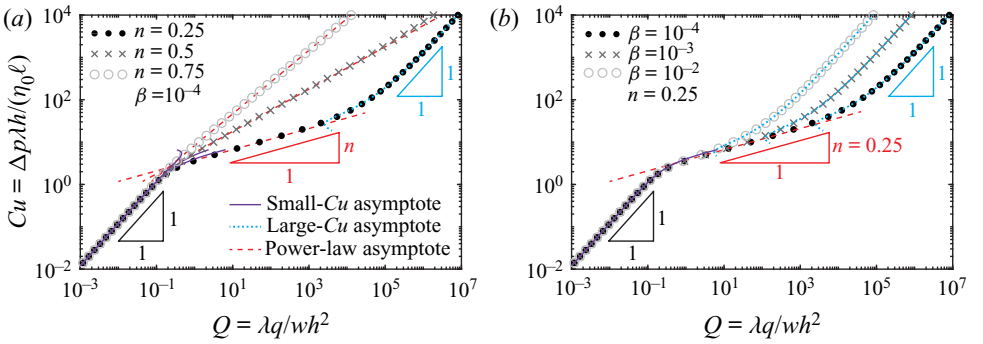

Figure 2. Theoretically predicted flow rate–pressure drop relation for the Carreau constitutive model in a straight channel. (*a*) Dimensionless pressure drop $Cu = \Delta p\lambda h/(\eta_0 \ell)$ vs flow rate $Q = \lambda q/(wh^2)$ for $n = 0.25, 0.5, 0.75$ and $\beta = 10^{-4}$. (*b*) Dimensionless pressure drop $Cu = \Delta p\lambda h/(\eta_0 \ell)$ vs flow rate $Q = \lambda q/(wh^2)$ for $\beta = 10^{-4}, 10^{-3}, 10^{-2}$ and $n = 0.25$. Dots, crosses and circles represent the semi-analytical results obtained by solving numerically (3.4) and (3.7). Purple solid and cyan dotted lines represent the asymptotic solutions (3.9) and (3.12) for $Cu \ll 1$ and $Cu \gg 1$, respectively. Red dashed lines represent the power-law asymptotic solution (3.10) for intermediate values of Cu.

We note that for $n = 1$, we have $\mathcal{H}_1 = 1 - \beta$ and $\mathcal{H}_2 = 0$, and $\eta/\eta_0 = \beta + Cu^{n-1}\mathcal{H}_1 + Cu^{2(n-1)}\mathcal{H}_2 + O(Cu^{3(n-1)})$ reduces to $\eta/\eta_0 = 1$, consistent with the Newtonian limit. In this case, however, the Taylor expansion $(\eta/\eta_0)^{-1} = \beta^{-1} - \beta^{-2}Cu^{n-1}\mathcal{H}_1 + \beta^{-3}Cu^{2(n-1)}(\mathcal{H}_1^2 - \beta\mathcal{H}_2)$, used to calculate (3.7), does not hold other than when $\beta = 1$, since $Cu^{n-1} = 1$ is no longer a small parameter. Therefore, for $n = 1$ (3.12) does not reduce to the Newtonian limit, $Q = Cu/12$, except in the case of $\beta = 1$. We also note that $\mathcal{H}_1 \propto Z^{n-1}$ and $\mathcal{H}_2 \propto Z^{2(n-1)}$ in (3.11*a*,*b*) have a singularity at $Z = 0$ for $0 < n < 1$. Nevertheless, since the first and second terms in the integrand of (3.7) are regular functions for $Z > 0$, and the third term $(\mathcal{H}_1^2 - \beta\mathcal{H}_2) \propto Z^{2n-1}$ has an integrable singularity, (3.7) can be calculated, resulting in (3.12).

We present the non-dimensional pressure drop $Cu = \Delta p\lambda h/(\eta_0 \ell)$ vs the flow rate $Q = \lambda q/(wh^2)$ in figure 2(*a*, *b*) for the Carreau model in a straight channel for different values of n and β. Dots, crosses and circles represent the semi-analytical results, whereas purple solid, red (- -) and cyan dotted lines represent the asymptotic solutions (3.9), (3.10) and (3.12) for small, intermediate and large values of Cu, respectively. To obtain the semi-analytical solution for given values of Cu, n and β, we first solved numerically (3.4) using MATLAB's routine fzero for η/η_0 as a function of $Z \in [0, 1/2]$, where Z was discretized with 201 points. Using the values for η/η_0, we integrated twice (3.7), first using MATLAB's routine cumtrapz to find the velocity profile and then using MATLAB's routine trapz to find the flow rate. We performed grid sensitivity tests by increasing the number of grid points to 301 and 401, resulting in a relative error below 10^{-5}, thus establishing grid independence. We note that alternative numerical approaches to calculating the $q-\Delta p$ relation of Carreau fluids were presented recently by Sochi (2015) and Wrobel (2020).

As expected, the results in figure 2(*a*) show that as the power-law index n characterizing the degree of shear thinning decreases, the $q-\Delta p$ relation transitions from the power-law to the large-Cu behaviour at smaller values of Cu for fixed values of β. Similarly, the results in figure 2(*b*) indicate that as the viscosity ratio $\beta = \eta_\infty/\eta_0$ decreases, the $q-\Delta p$ relation settles on the large-Cu linear behaviour at larger values of Cu for fixed values of n.

From figure 2(*a*, *b*), we see that there is excellent agreement between the semi-analytical results and asymptotic solutions over the entire range of values of the Carreau number. For $Cu \ll 1$, the asymptotic solution (3.9) accurately describes the behaviour of the $q-\Delta p$ relation up to Cu of $O(1)$ and captures well the transition to the power-law dependence $Q \approx Cu^{1/n}$, given in (3.10), for larger values of Cu. Furthermore, it is evident that the asymptotic solution (3.12) also accurately captures the transition from the power-law dependence (3.10) to the linear scaling $Q \sim Cu/(12\beta)$ for $Cu \gg 1$. We, therefore, conclude that the asymptotic solutions (3.9), (3.10) and (3.12) for small, intermediate and large values of Cu, which previously had been given for individual limits, accurately describe almost the entire range of values of the Carreau number. These approximate solutions can be directly compared with the $q-\Delta p$ experimental data without requiring any additional computations, provided that the rheological parameters are known.

4. Comparison with experiments and discussion

4.1. *Fit of viscosity data and rheological parameters of the Carreau model*

In this section, we compare the predictions of our theoretical analysis with the experimental results of Pipe *et al.* (2008), who measured the pressure drop of a shear-thinning xanthan gum solution in a slit microchannel for a wide range of flow rates (see their figure 14; unfortunately, there are misprints in the units of pressure in their figure 14, which should be in kPa and not Pa, as appears in table 2 of Pipe *et al.* (2008)). Using the Weissenberg–Rabinowitsch–Mooney equation (see e.g. Macosko (1994), p. 240), $\dot{\gamma}_w = (\dot{\gamma}_a/3)[2 + \mathrm{d}\ln\dot{\gamma}_a/\mathrm{d}\ln\tau_w]$, where $\dot{\gamma}_a = 6q/(wh^2)$, $\tau_w = \Delta p h/(2\ell)$ and $\dot{\gamma}_w$ is the *a priori* unknown shear rate. Pipe *et al.* (2008) converted the $q-\Delta p$ measurements into viscosity data through $\eta = \tau_w/\dot{\gamma}_w$ and by fitting the variation of $\ln\dot{\gamma}_a$ vs $\ln\tau_w$ with a second-order polynomial. In addition, Pipe *et al.* (2008) provided shear-rate-dependent viscosity data measured in cone-and-plate and parallel-plate rheometers.

Even though Pipe *et al.* (2008) presented the fit of the Carreau–Yasuda equation to the three viscosity data sets in their figure 17, no resulting rheological parameters were provided in their paper. However, such rheological parameters are essential for quantitative comparison between theory and experiments. Therefore, we reproduce the viscosity data of Pipe *et al.* (2008) in figure 3 and fit these to the Carreau equation to obtain these parameters; see table 1.

The viscosity data from Pipe *et al.* (2008) for aqueous xanthan gum solution, obtained from microchannel $q-\Delta p$ measurements and with cone-and-plate and parallel-plate rheometers, are shown in figure 3(*a*). The black line represents the fit of the Carreau equation (2.3) to the three data sets obtained using MATLAB's nonlinear least-squares routine lsqcurvefit (release R2020b, Mathworks, USA); the corresponding rheological parameters are provided in the upper row of table 1. It can be seen from figure 3(*a*) that cone-and-plate and parallel-plate rheometers provide viscosity data only for low and intermediate shear rates but are unable to capture the behaviour at high shear rates. This limitation of standard rheometers clearly highlights the importance of the microchannel flow measurements that allow us to assess the viscosity at intermediate and high shear rates. It is evident from figure 3(*a*) that for intermediate shear rates there is a significant discrepancy between the microchannel viscosity data and cone-and-plate and parallel-plate rheometer viscosity data, which significantly affects the values of the obtained rheological parameters. As we are interested in comparing the microchannel $q-\Delta p$ measurements with our theory, in figure 3(*b*) we present the fit of the Carreau model only to the microchannel rheological data and provide the resulting parameters in the lower row of

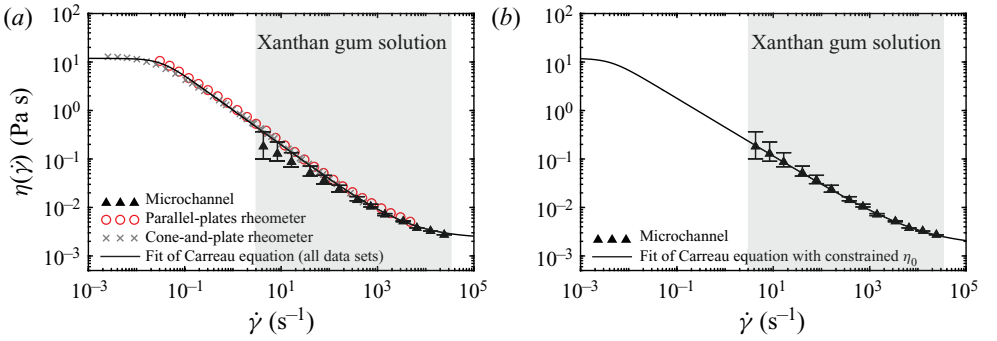

Figure 3. Experimental data from Pipe *et al.* (2008) and the fitting curves for viscosity as a function of shear rate for aqueous xanthan gum solution. (*a*) Fit of Carreau equation (—) to the complete set of parallel-plate (∘, red), cone-and-plate (×, grey) and microchannel (▲) data. (*b*) Fit of Carreau equation only to microchannel data with the constrained value of η_0 that matches the rheometer data at low shear rates. For clarity, the greyed-out regions in (*a*,*b*) indicate the range of shear rates corresponding to the microchannel data. The rheological parameters obtained from the fitting are summarized in table 1.

Rheological parameters	η_0 (Pa s)	η_∞ (Pa s)	β	n	λ (s)
Fitting to three data sets	11.9	2.31×10^{-3}	1.94×10^{-4}	0.279	30.4
Fitting to microchannel data set (with η_0 constraint)	11.9	1.61×10^{-3}	1.35×10^{-4}	0.402	239

Table 1. Rheological parameters obtained from fitting the viscosity dependence on the shear rate to the Carreau equation based on the complete data set (upper row) and based solely on microchannel data with the constrained value of η_0 (lower row).

table 1. While no microchannel rheological data are available for low shear rates, we expect the zero-shear-rate viscosity η_0 to attain the value obtained from rheometer measurements, i.e. $\eta_0 = 11.9$ Pa s, and thus in the fitting we constrain the zero-shear-rate viscosity to this value.

4.2. *Finite-length and finite-width effects*

Before making a quantitative comparison between theory and experiments, we summarize in table 2 the values of the physical parameters of the experimental system (microchannel A) of Pipe *et al.* (2008) used for the $q-\Delta p$ measurements of the shear-thinning xanthan gum solution. These values match well the assumptions of our theoretical analysis. In particular, we observe that $\epsilon = 1.94 \times 10^{-3}$ and $\delta = 7.94 \times 10^{-3}$, which satisfy $\epsilon \ll 1$, $\delta \ll 1$ and $\epsilon < \delta \ll 1$, although not strictly $\epsilon \ll \delta \ll 1$.

We note that the finite-length effect generated by entrance/exit flow disturbances, as commonly encountered in capillary rheometry, may affect the comparison between the theory and experiments and require some corrections (Macosko 1994). However, the experimental system of Pipe *et al.* (2008), which is schematically shown in figure 1, was designed to avoid such an effect by placing the pressure sensors far from the channel entrances and exits. Specifically, the distance between the inlet and the first sensor was $\ell_{in} = 2.025$ mm. As pointed out by Pipe *et al.* (2008), ℓ_{in} is equivalent to $42d_h$, where $d_h = 2hw/(h+w) \approx 48.2$ μm is the hydraulic diameter, and is significantly larger than the entrance length needed for fully developed flow at low Reynolds numbers. The distance

h (μm)	w (mm)	ℓ_{ch} (mm)	ℓ (mm)	Δp (kPa)
24.6	3.1	12.65	6.3 ± 1.6	$0.25 - 20.55$
q (μl min^{-1})	ϵ	δ	Cu	
$4.96 \times 10^{-2} - 3.94 \times 10^{2}$	1.94×10^{-3}	7.94×10^{-3}	$19.3 - 1618$	

Table 2. Values of the physical parameters for the experimental system (microchannel A) of Pipe *et al.* (2008), which measured the pressure drop Δp as a function of the flow rate q for the shear-thinning xanthan gum solution. The values of Cu are calculated taking η_0 and λ from the lower row of table 1, corresponding to the microchannel viscosity data.

between the last sensor and the outlet was $\ell_{out} = 4.325$ mm, which is even larger than ℓ_{in}. Therefore, at both points where the sensors measured the pressure, the flow was fully developed, and thus no correction is required.

Beyond the finite-length effect, an effect of the lateral sidewalls may also affect the comparison between the theory and experiments. However, as we show here, this effect is also negligible since $h/w \ll 1$. For small and large values of Cu, the viscosity is approximately constant, η_0 and η_∞, respectively, and the fluid behaves as Newtonian. To assess the finite-width effect for $Cu \ll 1$ and $Cu \gg 1$, we can therefore use the solution for the $q-\Delta p$ relation of the pressure-driven flow of a Newtonian fluid with viscosity η_0 in a three-dimensional channel, which is well approximated as $12\eta_0 \ell q/(wh^3\Delta p) = 1 - 0.627(h/w)$, yielding less than 10 % error for $h/w \leq 0.7$ (Stone 2007). We have $h/w = 7.94 \times 10^{-3}$, and thus effect of the lateral sidewalls is negligible for $Cu \ll 1$ and $Cu \gg 1$. For intermediate values of Cu, the fluid approximately behaves as a power-law fluid. Therefore, to assess the finite-width effect in this limit, we can use figure 5 from Middleman (1965) showing the parameter $S_p = q/wh^2(2\eta_0\lambda^{n-1}\ell/(h\Delta p))^{1/n} = Q(2/Cu)^{1/n}$ as a function of n for different values of w/h, obtained for the pressure-driven flow of power-law fluids in a three-dimensional channel. This figure shows that as the ratio w/h increases, S_p rapidly approaches the infinite-width limit $S_p = Q(2/Cu)^{1/n} = n/(4n+2)$, given in (3.10). For example, for $n = 0.5$ and $w/h = 4$ it follows that $S_p \approx 0.09$, whereas the infinite-width limit yields $S_p = 0.125$. In the experiments of Pipe *et al.* (2008), $w/h \approx 126 \gg 1$, and thus the effect of the lateral sidewalls is negligible for intermediate values of Cu as well.

4.3. *A quantitative comparison between theory and experiments*

We present in figure 4 a comparison of our semi-analytical and asymptotic solutions in dimensional form with the experimental measurements of Pipe *et al.* (2008) for the flow rate–pressure drop relation. We observe that when using the rheological parameters from a fit of the Carreau viscosity model to the three data sets shown in figure 3(*a*), our theory (red crosses) significantly overpredicts the experimental pressure drop (black triangles) for intermediate flow rates. We attribute this discrepancy to an apparent difference between the microchannel viscosity data and the cone-and-plate and parallel-plate rheometer viscosity data for intermediate shear rates (see figure 3*a*), which, as mentioned before, influences the values of the Carreau rheological parameters obtained from the fitting to all data sets. Hence, since we compare with microchannel $q-\Delta p$ measurements, we expect to obtain a much better agreement with experiments when using the rheological parameters corresponding to the fit of the Carreau viscosity model only to the microchannel data shown in figure 3(*b*).

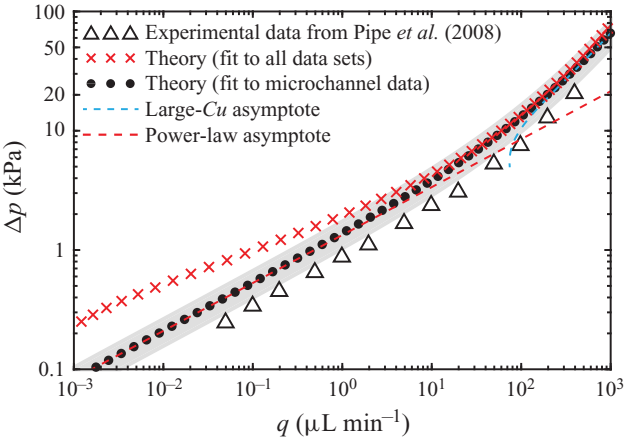

Figure 4. Comparison between our theory and the experimental data from Pipe *et al.* (2008) for the flow rate–pressure drop relation of xanthan gum solution. Triangles represent the experimental data and red crosses represent the theoretical results with the rheological parameters based on viscosity fitting to all data sets (table 1, upper row). Black dots represent the theoretical results, and red and cyan dashed lines represent the asymptotic solutions (3.10) and (3.12), with the rheological parameters based on viscosity fitting to the microchannel data set (table 1, lower row). A shaded trust region, based on taking $\ell = 6.3 \pm 1.6$ mm due to the axial size 0.8 mm of each pressure sensor that measured Δp in the experiments of Pipe *et al.* (2008), is included.

Black dots in figure 4 represent our semi-analytical solution, and red and cyan dashed lines represent the asymptotic approximations (3.10) and (3.12) with the rheological parameters from fitting the Carreau viscosity model to the microchannel data. Clearly, there is good agreement between our theoretical predictions and the experimental results. In particular, our theory captures the change in slope for high flow rates observed in experiments. As the asymptotic solutions (3.10) and (3.12) indicate, this change in the slope is associated with the transition from the power-law to the large-Cu behaviour with the linear leading-order $q-\Delta p$ relation, and cannot be predicted using a simple power-law model. Furthermore, we do not observe the transition from the low-Cu to the power-law behaviour in the experimental data shown in figure 4, since the microchannel $q-\Delta p$ measurements correspond to intermediate and large values of Carreau number, as follows from table 2. This is consistent with the microchannel viscosity data shown in figure 3(*b*), which indicates that the data are within the intermediate and high ranges of shear rates, as highlighted by the greyed-out region, and never reach the low-shear-rate viscosity plateau.

The theoretical results shown in figure 4 systematically overpredict the experimental pressure drop. One reason for this discrepancy is inherent uncertainty in the length ℓ over which the pressure drop measurements are performed, due to the finite axial size of 0.8 mm of each pressure sensor in the experiments of Pipe *et al.* (2008). We therefore added a shaded trust region, based on taking $\ell = 6.3 \pm 1.6$ mm, and obtained a much better agreement between theory and experiments. Finally, it is important to note that, unfortunately, Pipe *et al.* (2008) did not provide error bars for the $q-\Delta p$ measurements, thus making it difficult to draw conclusions about the relative error between the theory and experiments. Nevertheless, based on the microchannel viscosity data shown in figure 3(*b*), which are obtained from the $q-\Delta p$ measurements using a procedure briefly outlined in § 4.1 and characterized by large error bars at intermediate shear rates, one might also expect significant error bars in $q-\Delta p$ data for the intermediate flow rates.

5. Concluding remarks

Flow rate–pressure drop measurements of various non-Newtonian fluids in different geometries are widely conducted in the fluid mechanics and rheology communities. However, a comparison of experimental data with theory is rarely performed, presumably due to the difficulty of performing such a comparison when there is a lack of analytical expressions, even approximate ones, for the $q-\Delta p$ relation covering the entire range of pressures drops and flow rates. In this work, we demonstrated such a $q-\Delta p$ experiment/theory comparison for shear-thinning fluids, described by the Carreau rheological model, flowing in straight and long channels. We first presented a theoretical approach to calculating the flow rate–pressure drop relation in such geometries. In particular, we provided a semi-analytical expression for the $q-\Delta p$ relation and asymptotic solutions for small, intermediate and large values of the Carreau number that allow us to approximate analytically the entire flow rate–pressure drop curve. We then showed that our theoretical results can be directly used for a comparison with the experimental measurements of Pipe *et al.* (2008), finding excellent agreement between the two.

Our theoretical calculations, based on the Carreau model, rationalized the change in slope of the $q-\Delta p$ data of Pipe *et al.* (2008) at high flow rates (see figure 4), which cannot be explained using a simple power-law model. This fact clearly highlights the importance of quantitative comparison of theory or simulation with experimental data to provide insight into the adequacy of the constitutive model and values of the rheological parameters.

The presented theoretical approach is not restricted to the case of straight channels and can be readily utilized to calculate the flow rate–pressure drop relation of shear-thinning fluids in slowly spatially varying channels. For such channels, the fluid motion is still governed by the lubrication equations (3.1) to leading order in ϵ and δ, but the pressure gradient $\mathrm{d}p(x)/\mathrm{d}x$ is no longer constant and varies in the axial direction due to spatial variations of h and/or w. As a result, the viscosity distribution is not just z-dependent but also x-dependent, thus slightly modifying the subsequent analysis. Finally, while we analysed here the effect of the shear-thinning rheology on the $q-\Delta p$ relation, it is interesting to understand how other rheological properties, such as viscoelasticity, influence the flow rate–pressure drop relation in straight and non-uniform channels. This is left for future investigation.

Acknowledgements. We thank C.A. Browne, S.S. Datta, L.G. Leal and G.H. McKinley for helpful discussions.

Funding. This research was partially supported by the National Science Foundation through Princeton University's Materials Research Science and Engineering Center (DMR-2011750). E.B. acknowledges the support of the Yad Hanadiv (Rothschild) Foundation and the Zuckerman STEM Leadership Program.

Declaration of interest. The authors report no conflict of interest.

Author ORCIDs.
Evgeniy Boyko https://orcid.org/0000-0002-9202-5154;
Howard A. Stone https://orcid.org/0000-0002-9670-0639.

References

Anand, V., David, J. Jr. & Christov, I.C. 2019 Non-Newtonian fluid–structure interactions: static response of a microchannel due to internal flow of a power-law fluid. *J. Non-Newtonian Fluid Mech.* **264**, 62–72.

Bird, R.B., Armstrong, R.C. & Hassager, O. 1987 *Dynamics of Polymeric Liquids, Volume 1: Fluid Mechanics*, 2nd edn. John Wiley and Sons.

CARREAU, P.J. 1972 Rheological equations from molecular network theories. *Trans. Soc. Rheol.* **16** (1), 99–127.

CHRISTOV, I.C., COGNET, V., SHIDHORE, T.C. & STONE, H.A. 2018 Flow rate–pressure drop relation for deformable shallow microfluidic channels. *J. Fluid Mech.* **841**, 267–286.

DATT, C., ZHU, L., ELFRING, G.J. & PAK, O.S. 2015 Squirming through shear-thinning fluids. *J. Fluid Mech.* **784**, R1.

EWOLDT, R.H., JOHNSTON, M.T. & CARETTA, L.M. 2015 Experimental challenges of shear rheology: how to avoid bad data. In *Complex Fluids in Biological Systems* (ed. S.E. Spagnolie), pp. 207–241. Springer.

GUPTA, S., WANG, W.S. & VANAPALLI, S.A. 2016 Microfluidic viscometers for shear rheology of complex fluids and biofluids. *Biomicrofluidics* **10** (4), 043402.

HAPPEL, J.R. & BRENNER, H. 1983 *Low Reynolds Number Hydrodynamics*, 2nd edn. Martinus Nijhoff Publishers.

KANG, K., LEE, L.J. & KOELLING, K.W. 2005 High shear microfluidics and its application in rheological measurement. *Exp. Fluids* **38** (2), 222–232.

LODGE, A.S. & DE VARGAS, L. 1983 Positive hole pressures and negative exit pressures generated by molten polyethylene flowing through a slit die. *Rheol. Acta* **22** (2), 151–170.

MACOSKO, C.W. 1994 *Rheology: Principles, Measurements and Applications*. Wiley-VCH.

METZNER, A.B. 1957 Non-Newtonian fluid flow: relationships between recent pressure-drop correlations. *Ind. Engng Chem.* **49** (9), 1429–1432.

METZNER, A.B. & REED, J.C. 1955 Flow of non-Newtonian fluids—correlation of the laminar, transition, and turbulent-flow regions. *AIChE J.* **1** (4), 434–440.

MIDDLEMAN, S. 1965 Flow of power law fluids in rectangular ducts. *Trans. Soc. Rheol.* **9** (1), 83–93.

MOONEY, M. 1931 Explicit formulas for slip and fluidity. *J. Rheol.* **2** (2), 210–222.

MOROZOV, A. & SPAGNOLIE, S.E. 2015 Introduction to complex fluids. In *Complex Fluids in Biological Systems* (ed. S.E. Spagnolie), pp. 3–52. Springer.

MOUKHTARI, F.E. & LECAMPION, B. 2018 A semi-infinite hydraulic fracture driven by a shear-thinning fluid. *J. Fluid Mech.* **838**, 573–605.

PICCHI, D., ULLMANN, A., BRAUNER, N. & POESIO, P. 2021 Motion of a confined bubble in a shear-thinning liquid. *J. Fluid Mech.* **918**, A7.

PINHO, F.T., OLIVEIRA, P.J. & MIRANDA, J.P. 2003 Pressure losses in the laminar flow of shear-thinning power-law fluids across a sudden axisymmetric expansion. *Intl J. Heat Fluid Flow* **24** (5), 747–761.

PIPE, C.J., MAJMUDAR, T.S. & MCKINLEY, G.H. 2008 High shear rate viscometry. *Rheol. Acta* **47** (5-6), 621–642.

PIPE, C.J. & MCKINLEY, G.H. 2009 Microfluidic rheometry. *Mech. Res. Commun.* **36** (1), 110–120.

RABINOWITSCH, B. 1929 Über die viskosität und elastizität von solen. *Z. Phys. Chem.* **145** (1), 1–26.

SHAHSAVARI, S. & MCKINLEY, G.H. 2015 Mobility of power-law and Carreau fluids through fibrous media. *Phys. Rev.* E **92** (6), 063012.

SOCHI, T. 2015 Analytical solutions for the flow of Carreau and Cross fluids in circular pipes and thin slits. *Rheol. Acta* **54** (8), 745–756.

STONE, H.A. 2007 Introduction to fluid dynamics for microfluidic flows. In *CMOS Biotechnology* (ed. H. Lee, R.M. Westervelt & D. Ham), pp. 5–30. Springer.

SUTERA, S.P. & SKALAK, R. 1993 The history of Poiseuille's law. *Annu. Rev. Fluid Mech.* **25** (1), 1–19.

WROBEL, M. 2020 An efficient algorithm of solution for the flow of generalized Newtonian fluid in channels of simple geometries. *Rheol. Acta* **59** (9), 651–663.